

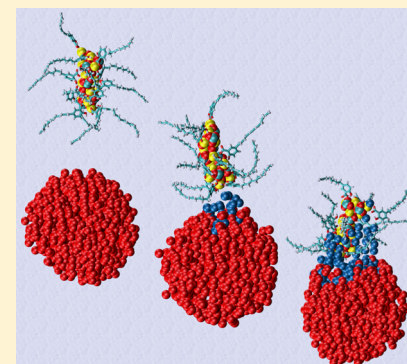
Response of Calcium Carbonate Nanoparticles in Hydrophobic Solvent to Pressure, Temperature, and Water

Michael S. Bodnarchuk,[†] David M. Heyes,[†] Angela Breakspear,[‡] Samir Chahine,[‡] Simon Edwards,[‡] and Daniele Dini*,[†]

[†]Department of Mechanical Engineering, Imperial College London, Exhibition Road, London, SW7 2AZ, United Kingdom

[‡]BP Technology Centre, Whitchurch Hill, Pangbourne, RG8 7QR, United Kingdom

ABSTRACT: Molecular dynamics simulations of surfactant-stabilized calcium carbonate, CaCO_3 , nanoparticles in hydrophobic solvent have been carried out to characterize their response to changes in temperature (T) and pressure (P) and also their interaction with trace water and water droplets. The response to increasing temperature and pressure is sensitive to the type of model surfactant, with the sulfonate-stabilized particle, which is the most spherical, showing a weak temperature-pressure dependence, while the sulfurized alkyl phenol and salicylate-stabilized particles distort into a more spherical shape with increasing temperature and pressure. The atom–atom radial distribution functions of the core ions reveal consolidation of the calcium carbonate structure with increasing temperature and pressure. The simulations show that the nanoparticles adsorb onto the surface of water droplets through a water bridge transitional mechanism, in agreement with evidence from experimental studies. In the case of the sulfonate surfactant particle only, a number of surfactant molecules detached from the calcium carbonate core and transferred to the surface of the water droplet. Consequently this type of particle had the greatest interaction with and affinity for water, which may explain its rapid neutralization characteristics observed in experiments. The detachment free energy of the sulfonate obtained by potential of mean force calculations was the largest of the three, which is consistent with the core being more embedded in the water and less well stabilized on returning to the hydrophobic medium. The salicylate nanoparticle had about half the detachment free energy, which could give rise to a more dynamic equilibrium of attached-to-detached states for this class of nanoparticle.



INTRODUCTION

Surfactant-stabilized calcium carbonate, CaCO_3 , nanoparticles are included in commercial engine oils to neutralize the acidic byproducts of combustion.¹ These so-called overbased detergents (ODs) are synthesized *in vivo* by a “one-pot” carbonation of lime in the presence of the surfactant.^{2–4} The structural properties of the OD have been extensively characterized by experiment^{5–7} and simulation^{2,3,8} under ambient laboratory conditions. These studies showed that the size and shape of the nanoparticle core depends on the type of surfactant and that they are typically $\sim 2\text{--}4$ nm across. There is evidence that the OD CaCO_3 core is at least partially amorphous.^{6,9–13} While these basic features of the OD particles are now well-characterized, their responsiveness to other components in the engine oil and changes in external conditions during operation are less well established. Their reaction to temperature and pressure changes is of interest, as engine temperatures can be ~ 150 °C and the pressure can be ~ 150 bar (in marine engines)^{14,15} under operating conditions. Very little is known about how temperature and pressure affect the OD particles and their influence on the OD neutralization reactivity. The interaction of the OD particles with water in the engine is of practical interest because water is likely to be the acid carrier.

The rate of neutralization increases with temperature,¹⁶ and by the addition of nonionic surfactants.¹⁷ There is evidence that the neutralization process is diffusion-controlled, with the merging of an acidic water droplet with the overbased particle being the rate-determining step,¹⁸ (presumably the neutralization of the calcium carbonate is then rapid and irreversible). The rate of reaction increases with temperature possibly because the number of water droplets increases with temperature by breakup of large droplets, so enhancing the probability of encounter with an OD particle.^{15,19,20} The surfactant molecules on the surface of the nanoparticle and the acid droplet can at least partially exchange on “collision”, exposing the CaCO_3 more effectively to the acid and subsequent neutralization.

The effects of increased pressure on OD particles have been less well studied. Fernandez-Martinez et al. showed that pure amorphous CaCO_3 is polyamorphic at pressures of many GPa.²¹ Our previous molecular dynamics (MD) simulations have concentrated on the effects of surfactant-type on the size and shape of the OD particle in hydrophobic solvent.^{2,3,8} This

Received: January 13, 2015

Revised: May 11, 2015

Published: May 27, 2015

work uses MD to explore their response to the environmental conditions of temperature, pressure, and trace water and water droplets that mimic some of the external conditions experienced by the OD nanoparticles during the operation of the engine.

SIMULATION DETAILS

Three different surfactant types were used to make the model the OD nanoparticles: (a) a sulfurized-alkyl phenol (SAP), (b) an alkyl-sulfonate, and (c) an alkyl-salicylate, whose chemical structures are given in Figure 1.

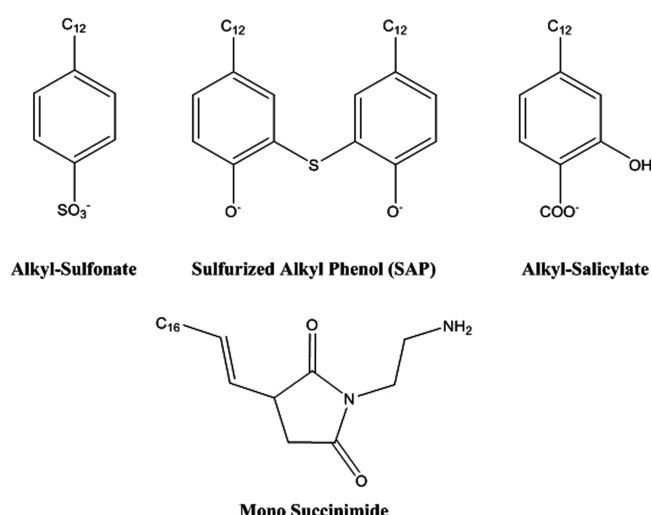


Figure 1. Three surfactant molecules used to make the OD nanoparticles (top row) and succinimide dispersant molecule (bottom row) used in this study.

The calcium and carbonate ions, and surfactant were initially randomly distributed in model cyclohexane in a periodic MD cubic cell. Over time these diffused together and an OD particle self-assembled, which was subsequently equilibrated by gradually reducing the ion charges and then returning them to their original values in two stages, as described in ref.^{8,22} The thermodynamic integration energy profile proved that in all cases the final state had a lower free energy than the initially formed particle. In the first set of simulations carried out here, the effects of increasing temperature and pressure are explored. In a second set of computations, a water droplet consisting of 1000 model water molecules and 40 nonionic succinimide surfactant molecules²³ was introduced into the system at a temperature of 300 K and pressure of 1 bar. The succinimides are used as dispersants in engine oil.

The quality of the force field is an important issue in any molecular simulation designed to reproduce the properties and phase behavior of specific chemical systems. The parameters for the succinimide molecules, cyclohexane and carbonate ions employed in this work were obtained from the online automated topology builder (ATB) server and used in the GROMOS53A6 force field.^{24,25} Classical potentials, such as the one used in this work, are capable of accurately predicting the properties of CaCO_3 containing systems in relation to a wide range of applications. For example, Tobias and Klein²⁶ investigated using MD the microscopic properties of a reverse micellar aggregate consisting of calcium carbonate, calcium (2-hexadecyl)benzenesulfonate, and water molecules in nonpolar solvents. Quigley and Rodger showed that CaCO_3 inside small, surfactant-stabilized nanoparticles is typically amorphous.¹¹ The following studies have used force fields with a similar form to the GROMOS53A6 force field to model calcium containing systems of some relevance to the present work. Kohagen et al.²⁷ showed that the simulations provide an accurate description of concentrated aqueous calcium chloride solutions when compared with neutron scattering and viscosity measurements. Wang and Becker²⁸ explored the thermodynamic stability of vaterite and kinetics of the orientational ordering of the carbonate ions. Jain et al.²⁹ simulated Ca^{2+} and PO_4^{3-} ions in water and observed the early stages of aggregation. Skovbjerg et al.³⁰ investigated the association of carboxylate surfactants in solution with a calcite surface. Reischl et al.³¹ modeled a calcium carbonate nanocluster at the end of a model atomic force microscopy (AFM) tip moving toward a calcite surface through water. These studies indicate that the present model gives as realistic a representation of the carbonate nanoparticle systems as is currently possible from available force fields.

Table 1 gives the number of species included in the simulations performed.

Simulations were performed using the MD simulation code, GROMACS v4.5.5.^{32,33} Each nanoparticle was simulated at three different pressures, 1, 80, and 150 bar, and at six different temperatures, 300, 350, 400, 450, 500, and 550 K. In each case an MD equilibration simulation of 1 ns length in the NPT ensemble was performed prior to each production simulation. The particle mesh Ewald method³⁴ was used to compute the electrostatic terms in the potential, with interactions between atoms within 1.0 nm evaluated every time step and every five steps for atom pairs further apart. The nonbonded van der Waals terms were modeled using the Lennard-Jones pair potential with a cutoff of 1.2 nm. Verlet's leapfrog equation of motion integrator was used with a time step of 2 fs. The bond distances and angles of water molecules were constrained using the SETTLE algorithm³⁵ and all other bonds applied using LINCS.³⁶ Temperature was regulated using a velocity rescaling

Table 1. Summary of the Molecular Details of the Simulations, Including the Number of Each Species Used in the Simulations^a

system	surfactant	cyclohexane	calcium	carbonate	water	succinimide
SAP	6	1361	16	10	0	0
sulfonate	12	1680	16	10	0	0
salicylate	12	1649	16	10	0	0
SAP + droplet	6	4067	16	10	1000	40
sulfonate + droplet	12	4035	16	10	1000	40
salicylate + droplet	12	4150	16	10	1000	40

^aTop three rows are for the temperature and pressure variation sets of simulations. bottom three rows refer to the simulations carried out with a single nanoparticle and single water droplet.

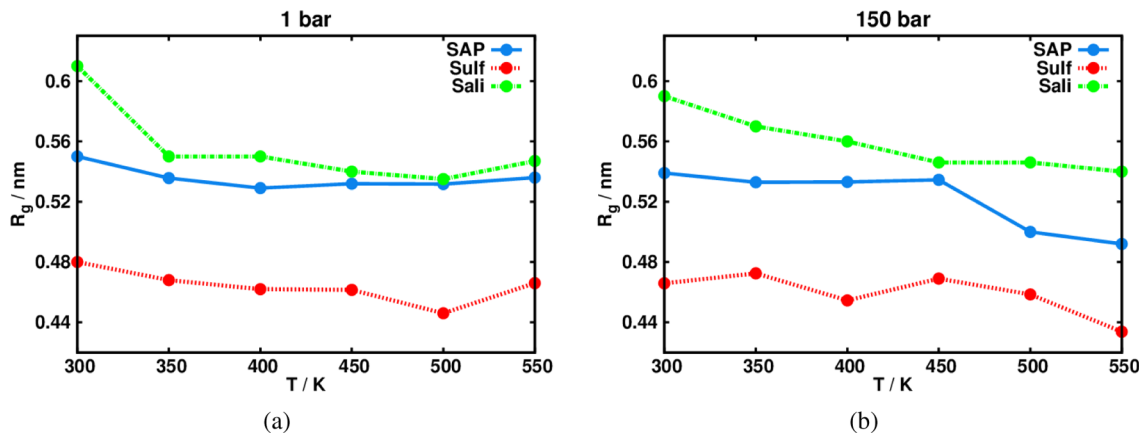


Figure 2. Radius of gyration at 1 bar (frame a) and at 150 bar (frame b) for the three surfactant-stabilized nanoparticles.

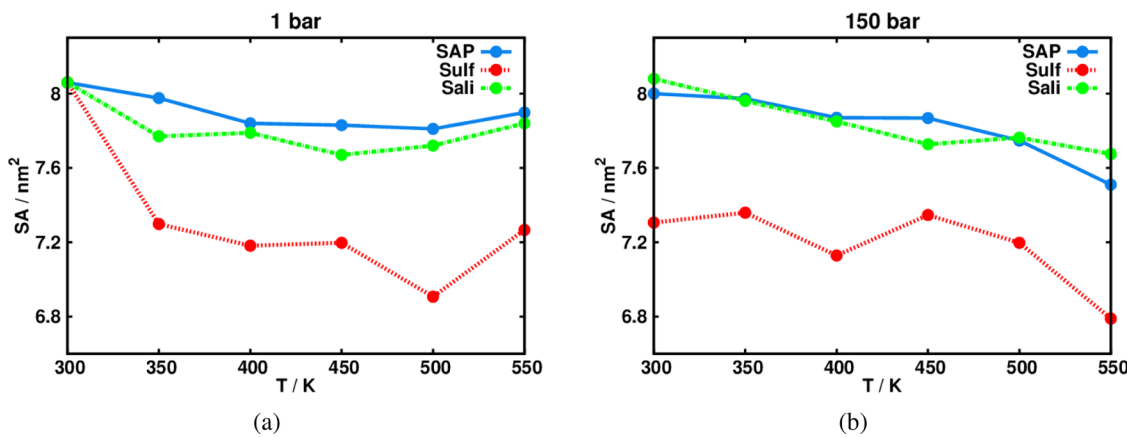


Figure 3. Accessible surface area at 1 bar (frame a) and at 150 bar (frame b) for the three surfactant-stabilized nanoparticles.

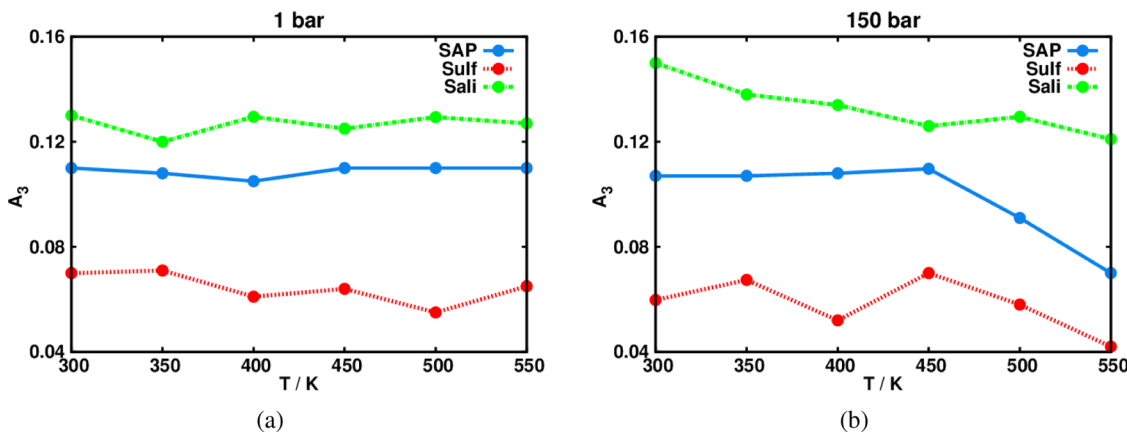


Figure 4. Asphericity of the CaCO_3 core at 1 bar (frame a) and at 150 bar (frame b) for the three surfactant-stabilized nanoparticles.

thermostat with a coupling time of 0.1 ps,^{37–39} and the external pressure was set using the Parrinello–Rahman barostat.⁴⁰ Each simulation was performed for 20 ns in the NPT ensemble, with data collected over the last 5 ns. Structural analysis was performed using the inbuilt GROMACS packages g_sas, g_gyrate, g_dist, and g_rdf. The shape of the nanoparticle was determined using a literature asphericity order parameter, A_3 ,^{41,42} derived from the moment of inertia tensor which was accumulated during the simulation as follows

$$A_3 = \frac{\langle \sum_{i \neq 1} (\lambda_i - \lambda_1)^2 \rangle}{2 \langle (\sum_{i=1}^3 \lambda_i)^2 \rangle} \quad (1)$$

where $\langle \dots \rangle$ denotes a time average and λ_i are the principle moments of inertia of the core or total nanoparticle. A value of $A_3 = 0$ indicates a sphere and 0.25 indicates an infinitely thin circular disk.

RESULTS AND DISCUSSION

First, the effects of temperature and pressure on the shape and core ion organization are considered.

Temperature and Pressure Effects. Figures 2–4 present the radius of gyration, R_g , the solvent-accessible surface area, SA, and the asphericity, A_3 , respectively, for the SAP, sulfonate, and salicylate nanoparticles as a function of temperature for an external pressure of 1 bar (lefthand frame, a) and 150 bar (righthand frame, b). Frames (a) and (b) of Figure 2 indicate that the radius of gyration of the three nanoparticles gradually decreased with increasing temperature, with the effect being more pronounced at 150 bar.

The accessible surface-area profiles in Figure 3 show a slight reduction with temperature at 1 bar for the SAP and salicylate OD particles, with the sulfonate nanoparticle experiencing a large decrease in accessible surface area between 300 and 350 K. At 150 bar there is a larger reduction in the accessible surface area with increasing temperature for the SAP and salicylate cases, which correlates well with the decrease in R_g shown in Figure 2.

Figure 4 shows the asphericity parameter for the three nanoparticles as a function of temperature for pressures of 1 bar (frame (a)) and 150 bar (frame (b)). At 1 bar, the sulfonate particle becomes slightly more spherical with increasing temperature. The OD particle formed from the other two surfactant types shows no statistically significant change in A_3 with temperature. All OD particles become more spherical with temperature at 150 bar, especially above 450 K for the SAP and salicylate OD particles, which is consistent with thermodynamics, as the associated reduction in surface area reduces the surface tension contribution to the free energy.

To assess the stability of the structures formed at the higher temperatures and pressures, we simulated each nanoparticle for a further 5 ns. The properties and configurational energies were statistically the same after this time scale, indicating that no significant further restructuring of the nanoparticle had occurred. The differences in the configurational energies at high and low temperatures were found to be statistically significant, indicating that the nanoparticles are not metastable and instead reflect the conditions upon which they are simulated. The nanoparticles formed at temperatures greater than 450 K and 80 bar were additionally quenched to 300 K and 1 bar, and the simulations continued for a further 10 ns. Both R_g and the surface area increased during this time, as expected, as the nanoparticles rearranged to a lower free energy consistent with the new temperature and pressure. There was a small difference in the properties and configurational energy of the relaxed structure compared with the original structures formed at 300 K and 1 bar.²² It would be surprising if there was no hysteresis at all, as the original trajectory through phase space is not reversed and species will finally adopt different positions with slightly different structures with almost the same free energy. (The free-energy profile is likely to be relatively flat with many slightly different structures having almost the same lowest free energy.) Within the framework of the computer model and the capacity of our computational resources, it can be concluded, nevertheless, that the main features of the structures formed at the various temperatures and pressure modeled here are statistically significant thermodynamically favored states.

Figures 2–4 indicate that the salicylate nanoparticle becomes more compact and slightly less elongated with increasing temperature and pressure, which is evident also in the two atomic snapshots given in Figure 5. The distance between the two highlighted calcium ions is smaller at higher temperature.

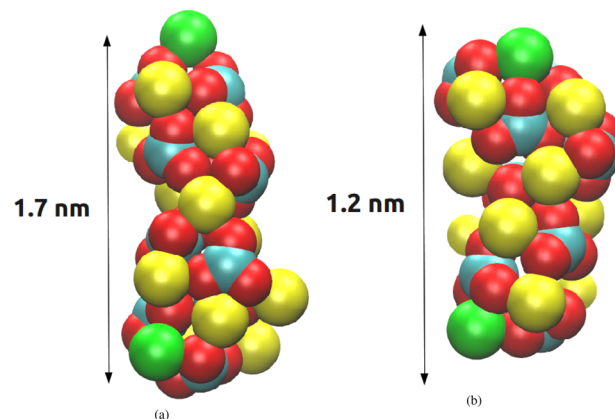


Figure 5. Snapshots of the cores of a salicylate-stabilized nanoparticle at (a) 300 and (b) 550 K at a pressure of 150 bar. The distance between the two calcium ions shown in green is given on the Figure for each temperature. The remaining calcium ions are shown in yellow. The cyan and red spheres represent the carbon and oxygen atoms, respectively, of the carbonate ions.

Figure 6 shows that the height of the first peak for the Ca–Ca and Ca–O RDFs increases with temperature for the salicylate nanoparticle. The Ca–Ca first peak gradually transforms from two poorly defined peaks into one. The second peak Ca–Ca in Figure 6a at ≈ 0.60 nm splits into two overlapping peaks at 550 K, with the center of the peaks being at approximately the same distance as the original peak at 300 K. There is only a small increase in the Ca–O pair intensities with increasing temperature. The second of the split second peak at $r \approx 0.40$ nm becomes more intense at 550 K.

Phase changes in bulk calcium carbonate take place at high temperature and pressure. Fernandez-Martinez et al.²¹ discovered using X-ray diffraction so-called “aragonitic” amorphous calcium carbonate, which formed at high pressure (>20 GPa). The Ca atoms adopted a local order similar to bulk aragonite but retained some amorphous structural characteristics, notably the center of broad Ca–Ca peaks at ≈ 0.58 nm in the amorphous structure coincides with the center of two peaks in aragonite.

Bulk calcite and aragonite were simulated using the nanoparticle force field employed here. The radial distribution functions (RDF) for bulk calcite and aragonite were calculated from a 5 ns MD simulation at 300 K at a pressure of 1 bar. The positions of the radial distribution peaks are given in Table 2, together with the RDF peak positions of the surfactant-stabilized calcium carbonate nanoparticles. The peak positions found from a previous MD study of bulk CaCO_3 phases by Bearchell et al.⁴³ are also given in Table 2. The two sets of bulk RDF data are statistically the same. The small standard deviations in the peak positions for the bulk phases modeled here indicate that these two CaCO_3 phases are stable using the nanoparticle force field.

Table 2 shows that the SAP and salicylate nanoparticles display the presence of possible “aragonitic” Ca–Ca peaks at ≈ 0.58 nm, suggesting deviation from a purely amorphous structure. In addition, the RDF details given in Table 2 show that the core of the nanoparticles in the high temperature and pressure limit exhibits some features that are closer to aragonite than calcite (i.e., the split second peak in Ca–Ca and Ca–O RDFs at ~ 0.55 nm, which corresponds to the third peak in aragonite); however, there is no second peak at 0.49 (calcite) or

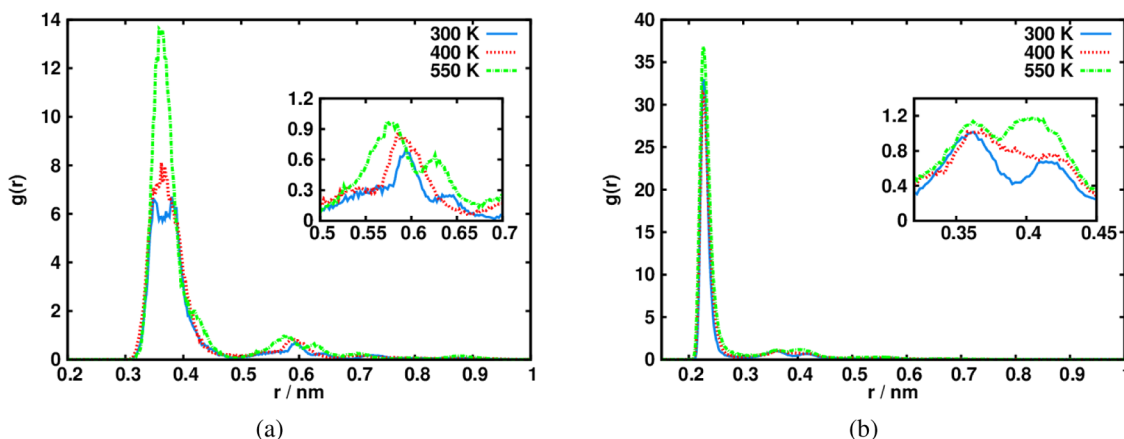


Figure 6. Radial distribution functions (RDF) for (a) the Ca–Ca ion pair and (b) the Ca–O pair as a function of temperature for the salicylate-stabilized nanoparticle at 150 bar. Regions of interest for the RDFs are shown in inserts.

Table 2. Positions of the First Three Radial Peaks for the Ca–Ca and Ca–O Pairs in Bulk Calcite and Aragonite Structures Found from a MD Simulation (-MD) Compared with Those of the Simulated Nanoparticles at 550 K and 150 bar^a

structure	$g_{\text{Ca}-\text{Ca}}$ (r)/nm			$g_{\text{Ca}-\text{O}}$ (r)/nm		
	peak 1	peak 2	peak 3	peak 1	peak 2	peak 3
calcite-MD	0.38(0.01)	0.49(0.02)	0.65(0.01)	0.23(0.02)	0.37(0.00)	0.44(0.02)
calcite-B	0.40	0.50	0.64	0.24	0.34	0.42
aragonite-MD	0.38(0.02)	0.45(0.02)	0.57, 0.61(0.01)	0.23(0.02)	0.41, 0.44(0.02)	0.53(0.01)
aragonite-B	0.39	0.46	0.57, 0.62	0.25	0.41, 0.43	0.53
SAP	0.36		0.57, 0.63	0.23	0.36, 0.41	0.55
sulfonate	0.38		0.59	0.23	0.37, 0.42	0.57
salicylate	0.37		0.58, 0.63	0.23	0.38, 0.42	0.56

^aPrevious MD data of pure calcite and aragonite is shown for comparison (-B).⁴³ Standard deviations are shown in parentheses and calculated after removing the data from the first 1 ns of the MD simulation for equilibration.

0.45 nm (aragonite), so the OD atomic structures cannot be calcite or aragonite. Because of the small number of ions in the core, surface-to-volume and particle shape effects may have a significant impact on the microstructure, which appears to take on a form that is neither of the two most common bulk forms of calcium carbonate.⁴⁴

To conclude, on the basis of these simulations, the high T and P conditions found in marine engines should be sufficient to change the size and shape of the OD nanoparticles. The salicylate OD particles especially decrease in size and become more spherical at the higher pressure considered. This is consistent with thermodynamics as the contribution to the free energy of the particle from the surface tension, γ , term will then be minimized. In fact, the role of surface tension in determining the properties of the OD nanoparticles has perhaps not been sufficiently considered to date. Assuming $\gamma \approx 200 \text{ mN m}^{-1}$ ⁴⁵, the internal pressure acting on the core due to surface tension and using Laplace's equation is $\sim 1 \text{ GPa}$, which is considerably higher than the applied external pressure, so it could have a major indirect effect on the OD particle's structural characteristics and reactivity.

Atomistic simulations of stress in titania nanoparticles⁴⁶ showed that even quite large internal pressures on the order of 1 GPa are present for a nanoparticle diameter of 3 nm. (See figure 3 in that paper.) Therefore, it is apparent that Laplace's equation provides an accurate measure of the internal pressure in this size region (which is the same diameter region as for the carbonate nanoparticles simulated here). In fact, our prediction

of a 1 GPa internal pressure is in complete agreement with the prediction from ref 46.

NANOPARTICLE AND TRACE WATER

ODs rarely exist in purely hydrophobic environments, and there is typically at least trace water in the solvent. Umbrella sampling was used to calculate the free energy of dissociation between an OD particle and a single water molecule absorbed on its surface.⁴⁷ The water molecule was pulled along one direction, defined as the z axis, over a period of 1 ns, using a spring constant of 500 kJ mol⁻¹ nm⁻² and a separation withdrawal rate of 0.01 nm ps⁻¹. Approximately 100 equally spaced initial starting configurations were chosen, and in each window, MD was performed for 10 ns in the NPT ensemble (using a temperature of 300 K and pressure of 1 bar). The weighted histogram analysis method (WHAM) was used.⁴⁸ Figure 7 presents PMF profiles for the three surfactant nanoparticles, generated by restraining the position of the OD and pulling the water molecule away until the attractive force was statistically zero.

The Figure shows that the three surfactants generate very different PMF profiles. The dissociation free energy (the limit on the far right of the Figure) is almost the same ($\approx 28k_{\text{B}}T$) for the SAP and sulfonate-stabilized nanoparticle, although the intervening free-energy landscape is quite different between the two. More peaks and troughs are seen for the SAP nanoparticle, indicating a larger number of local minima on the nanoparticle surface than for the sulfonate. Two structures derived from the nanoparticle simulations are shown within the Figure to help

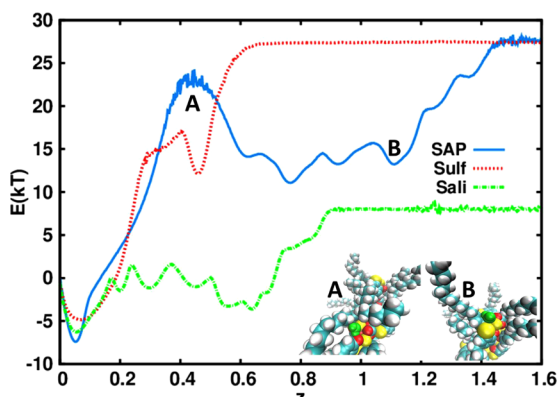


Figure 7. PMF free-energy profiles for the dissociation of a single water molecule from each type of surfactant stabilized nanoparticle. Inserts A and B show some of the local minima and maxima for the SAP nanoparticle. Calcium ions are shown as yellow spheres, the water molecules are shown as green spheres, and the carbon and oxygen atoms, respectively, of the carbonate ions are shown as cyan and red spheres.

explain the origins of the peaks and troughs in the PMF profiles. Structure A (corresponding to SAP curve peak labeled, A) is where the water molecule becomes trapped between the core and the surfactant tail. Structure B, corresponding to the local minimum, B, of the SAP profile is where the water molecule is at the solvent-accessible face of the core. Therefore, as the water molecule passes over the nanoparticle, it can get trapped in between the CaCO_3 core and the surfactant tail, which results in a large increase in the PMF energy due to the repulsive interactions between the hydrophobic tail and the water molecule. The water molecule can be found near the solvent-exposed region of the nanoparticle, shown in the right insert (B) of Figure 7, which results in a favorable local minimum energy.

The salicylate-stabilized nanoparticle does not interact with the water molecule as strongly as the other two surfactant types as the dissociation free energy is much smaller ($\approx 8 k_{\text{B}}T$). The landscape has a large number of possible local minima on the surface, suggesting that the water molecule might not get as close to the core as in the sulfonate and SAP-stabilized nanoparticle cases. The probability of a water molecule become detached from the core by thermal motion is proportional to $\exp(-E/kT)$, and based on the profiles in Figure 7 there is an extremely small probability of water detachment at room temperature. Therefore, the OD particles have a great affinity for trace water and will scavenge up any trace amounts from the hydrophobic solvent.

NANOPARTICLE–WATER DROPLET ASSOCIATION

The rate-determining step for the neutralization of an acid droplet by an overbased particle is thought to be the diffusing together and adsorption of the overbased particle on the surface of a water droplet in the oil.^{17,18} A water bridge can then form, during which the neutralization process can proceed. To discover if this proposed pathway is realistic, we performed MD simulations of an OD nanoparticle and a water droplet of similar size in the same MD simulation cell. The water droplet contained 1000 explicit water molecules represented by the SPC potential, which was immersed in explicit cyclohexane solvent. Being a classical model, the neutralization process itself cannot be followed by this MD technique, and there is no acid

in the present model, but these simulations can still give insights into the structural aspects of the reaction mechanism pathway and its sensitivity to surfactant type.

At least five independent simulations were performed for each class of nanoparticle, with different starting positions at 300 K and 1 bar. For each surfactant type only about one simulation in five encounters of the two particles produced a merged nanoparticle–water droplet system. In the other four cases the two particles diffused away again, indicating that the relative orientation of approach is an important factor in determining successful “capture”. The nonionic succinimide surfactant molecules did not associate with either the water droplet or the overbased particle to any great extent and stayed in the bulk for most of the simulation. Representative snapshots for the salicylate, SAP, and sulfonate-based nanoparticles as they merge with the water droplet are shown in Figures 8–10, respectively.

The sequence of snapshots frames in Figures 8–10 supports the diffusion-controlled neutralization mechanism proposed by Wu et al.^{17,18} that the mutual diffusion of the OD nanoparticle

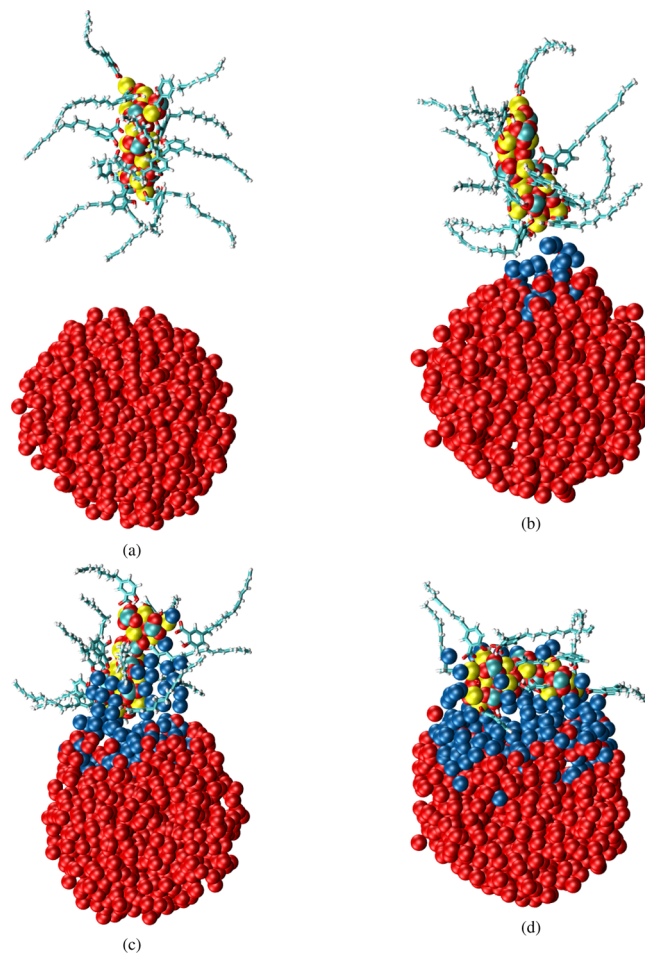


Figure 8. MD snapshots during a 20 ns simulation of a salicylate nanoparticle and a representative water droplet, showing the successive stages of (a) preassociation, (b) formation of an intermediate state, (c) development of a bridge between the two particles, and (d) the nanoparticle stably adsorbed on the surface of the droplet. Water molecules within 7 Å of the nanoparticle are shown as blue spheres, with the rest represented by red spheres. Calcium ions are shown in yellow. The cyan and red spheres represent the carbon and oxygen atoms, respectively, of the carbonate ions.

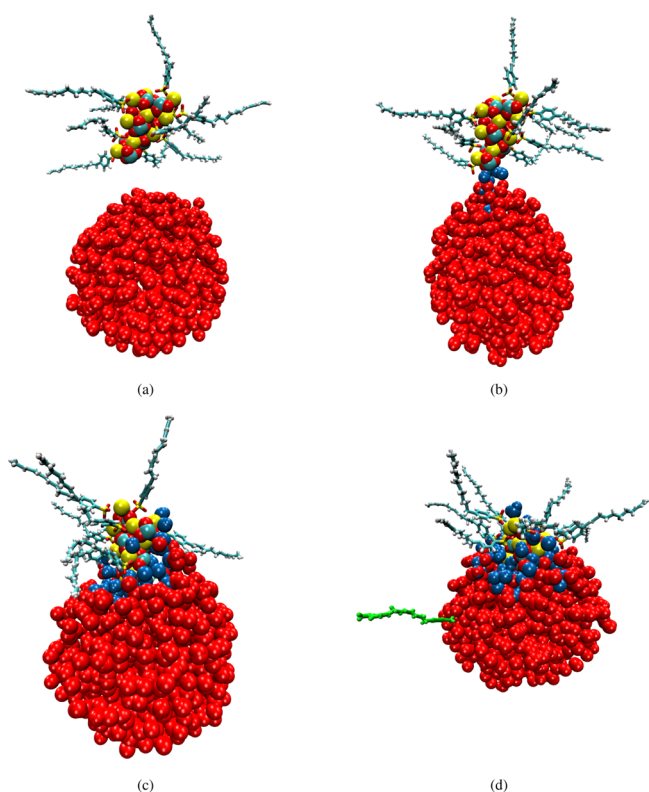


Figure 9. As for Figure 8, except the behavior of the SAP nanoparticle is shown.

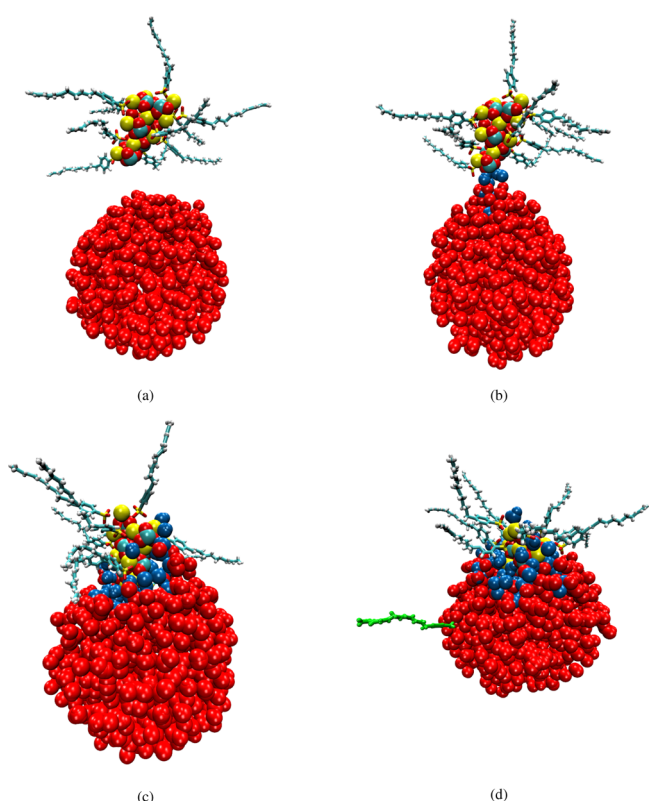


Figure 10. As for Figure 8, except the sulfonate nanoparticle behavior is shown.

and water droplet through the solvent is probably the rate-determining step. Successful merging of the OD nanoparticle

with the water droplet occurs when the polar core of the overbased particle is very close to but not necessarily touching the water droplet and while the hydrophobic tails of the surfactant remain immersed in the hydrophobic solvent. The OD particle is stable at the oil–water interface, as is in fact already known from Langmuir trough experiments on these systems.⁴⁹ Surface adsorption of emulsion droplets by colloidal particles (“Pickering” emulsions,^{50,51}) is known to provide a stabilizing mechanism for emulsions. Indeed, these nanoparticles may act to join two droplets together by a “bridging” mechanism, which may explain the experimental evidence for “aggregation” of OD particles in hydrophobic solvent,⁵² which may in fact be the aggregation of the water droplets through OD nanoparticle linkages.⁵²

Figures 8 and 9 for the SAP and salicylate OD cases show that the first stage of the association involves the nanoparticle approaching the droplet in an orientation, which puts the majority of the CaCO_3 close to the water (see frame (a)). The parts of the core that have less base in the middle of the OD nanoparticle do not interact strongly with the water. In contrast, the sulfonate-based nanoparticle has a reduced orientational dependence in this regard as it is more isotropic and compact. This may result in an entropic barrier to overcome for SAP and salicylate-based nanoparticles during the association process, which may result in decreased rates of neutralization. When the two species become close, water molecules from the droplet move toward the nanoparticle by electrostatic attraction from the core calcium ions to the polar water molecules (see frame (b)). More water molecules then attach onto the nanoparticle surface to create a channel via which the acid (were it present) could cross (in frame (c)), which can be seen on the right-hand side of the nanoparticles in Figures 8 and 9. In the last stage, the nanoparticle fully adsorbs onto the surface of the water droplet (visible in frame (d)), where a neutralization reaction could proceed relatively rapidly.

Figure 10 shows that the sulfonate nanoparticle interacts with the water droplet quite differently from the SAP and salicylate cases. On association, some of the sulfonate surfactant molecules (shown in green) detach from the CaCO_3 core and transfer to stabilize the water droplet instead. The sulfonate CaCO_3 core penetrated deeper into the water droplet than was the case for the other OD particles made up of the two other surfactant examples. In a previous publication we showed that sulfonate surfactants do not penetrate into the CaCO_3 core as much as SAP and salicylate surfactants,⁸ so it is reasonable that they will be more readily displaced during the adsorption onto the water surface. The SAP and salicylate headgroups are more embedded within the core, and therefore detachment onto the water droplet surface is less favorable. Fu et al.^{15,20} suggested that surfactant molecules are able to detach from an overbased core to facilitate and enhance the neutralization process, which our simulations support, at least for the sulfonate. Sulfonate OD nanoparticles have been shown by experiment to exhibit faster neutralization rates reaction rates than the salicylate and SAP-based analogues,^{53,54} and our simulation results indicate that this may be due to greater core–water interfacial area once adsorbed.

The free energy of association between a droplet and a nanoparticle cannot be determined by conventional MD, although the reverse process can. Umbrella sampling was used to generate a potential of mean force (PMF) or dissociation free energy for each particle pair.⁴⁷ The nanoparticle was pulled away from the water droplet along one

direction (the z axis) over a period of 1 ns, using a spring constant of 2000 $\text{kJ mol}^{-1} \text{nm}^{-2}$ and a pulling rate of 0.01 nm ps^{-1} . Approximately 200 equally spaced initial starting configurations were chosen, and in each window MD was performed for 10 ns in the NPT ensemble (using a temperature of 300 K and pressure of 1 bar). The total simulation time across all windows was 2 μs . The WHAM was used.⁴⁸

Figure 11 presents PMF profiles for the three surfactant-nanoparticles, generated by restraining the center of mass of the

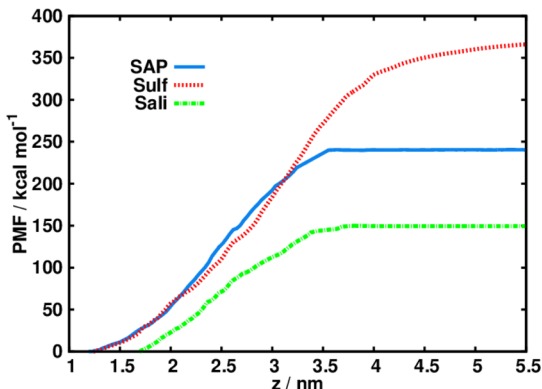


Figure 11. PMF free-energy profiles for the dissociation of surfactant-stabilized nanoparticles from a water droplet.

water droplet and pulling the nanoparticle away until the attractive force was statistically zero.

Figure 11 shows that the three surfactants have very different PMF profiles. The salicylate-based nanoparticle has the lowest detachment free energy of the three surfactants, probably because this nanoparticle penetrated the droplet to the least extent (as may be seen in Figure 8).

The sulfonate-based nanoparticle has the highest free energy of dissociation, indicating that the strength of attraction between the OD particle and the droplet is the strongest, as several of the sulfonate molecules had already transferred from the calcium carbonate core to the surface of the droplet. The detached particle after the pulling off would be less than optimally thermodynamically stable, hence the high detachment free energy. This nanoparticle also starts by being more buried into the water droplet and therefore has a greater number of favorable interactions between the core ions and the water than is the case for the other two surfactant molecules. The strong degree of association of the sulfonate is also consistent with the rapid neutralization characteristics of the sulfonate-based OD compared with salicylate and SAP cases.⁵⁴ The sulfonate PMF profile rises more gradually than those of other surfactant types, which form plateaus at a separation of ca. 3.5 nm. The salicylate and SAP-based nanoparticles begin to show convergence after 3.5 nm, while the sulfonate nanoparticle only begins to converge after 4.5 nm. In fact, the snapshot in Figure 12 reveals that the CaCO_3 core of the sulfonate nanoparticle became stretched out along the z direction as it was pulled away from the droplet. The relatively strong electrostatic attraction between the core and water droplet could be the origin of this stretched-out core.

It is well-established from Langmuir trough experiments that OD nanoparticles have a strong affinity for being at the water-air interface, with a contact angle of $\sim 90^\circ$.^{2,49} The detachment free energy is (apart from an $O(1)$ constant) $\approx \gamma A$, where A is the area of the water surface occupied by the nanoparticle,

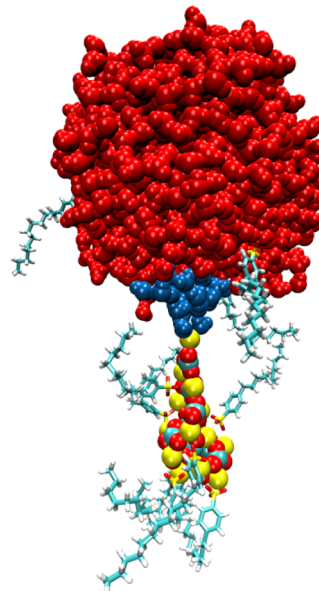


Figure 12. MD snapshot showing the stretching of the sulfonate-stabilized CaCO_3 core on dissociation from the water droplet.

which gives pull-off free energies comparable to those produced by the present PMF calculations.

CONCLUSIONS

Any molecular simulation study of a chemical system is limited by the software and computational resources available at a given time. In the previous simulation work on model oil soluble surfactant-stabilized calcium carbonate nanoparticles (model “overbased detergents” used in automotive and marine engine oils) carried out in the 1990s only single particles could be modeled in a small solvent molecule or effective solvent. We recently reported a more systematic examination of the structural properties of these particles in more realistic model solvents including water.⁸ This ambition of modeling more realistically the experimental systems is continued here.

The present molecular simulation study has demonstrated that calcium-carbonate-overbased nanoparticles become smaller and more spherical at the elevated pressures and temperatures encountered in automotive and marine engines. This could have implications for their chemical reactivity which should be taken into account in quantum mechanical studies (the internal pressure from surface tension effects can be on the order of 1 GPa). The arrangement of the ions in the core appears to be largely amorphous but nevertheless shares some features in common with so-called bulk “amorphous aragonitic”, which calcium carbonate forms at high pressures. The influence of the large surface-to-volume ratio on the core structure still appears to be not well understood and would benefit from further investigation.

The interaction of the nanoparticles with water is investigated further here. The “pull off” free energy of water molecules from the carbonate core is $\sim 30 k_B T$ for all surfactant types, which provides further evidence of the high affinity of these particles for water. This suggests that any trace water in a hydrophobic solvent will eventually by diffusion adhere to the carbonate cores. The MD simulations of nanoparticle adsorption onto a water droplet are the first of their kind and give support for the neutralization mechanism proposed by Fu and coworkers,^{15,20} which involves some surfactant (in the

sulfonate case) transferring onto the water overbased particle, which would surely increase the neutralization rate.⁵⁴ Potential of mean force, PMF, calculations indicate that the detachment free energy of the nanoparticle is greatest for the sulfonate and least for the salicylate, suggesting that the former particles will be the fastest to react.

These are the first molecular simulations to be reported of the coupling mechanism between the inverse micelle calcium carbonate nanoparticles (NP) in hydrophobic solvents with water droplets. The PMF figures reveal the way in which the NP approaches the water droplet, which could (ultimately) provide an understanding of some aspects of the acid neutralization mechanism for different surfactant stabilizers. They show that the anisotropic SAP/salicylate NPs have a higher entropic barrier to overcome than the sulfonate cases, as they need to approach "end-on" toward the water droplet to be captured. They are therefore inherently less reactive than the sulfonates.

The favorable interactions between the nanoparticles and the water droplet suggest that they could act in some sense as "Pickering" microemulsions and give rise to water droplet aggregation in hydrophobic solvent (the nanoparticle joining two water droplets together).⁵² Circumstantial evidence of this was discovered in ref 52.

AUTHOR INFORMATION

Corresponding Author

*E-mail: d.dini@imperial.ac.uk.

Notes

The authors declare no competing financial interest.

ACKNOWLEDGMENTS

M.S.B. thanks BP R&M Lubricants, Marine Technology (Pangbourne) for funding his Postdoctoral Research Fellowship to carry out this work.

REFERENCES

- (1) Lee, C. L.; Dowding, P. J.; Doyle, A. R.; Bakker, K. M.; Lam, S. S.; Rogers, S. E.; Routh, A. F. The Structures of Salicylate Surfactants with Long Alkyl Chains in Non-aqueous Media. *Langmuir* **2013**, *29*, 14763–14771.
- (2) Griffiths, J. A.; Bolton, R.; Heyes, D. M.; Clint, J. H.; Taylor, S. E. Physico-chemical Characterisation of Oil-soluble Overbased Phenate Detergents. *J. Chem. Soc., Faraday Trans.* **1995**, *91*, 687–696.
- (3) Bearchell, C.; Danks, T.; Heyes, D. M.; Moreton, D. J.; Taylor, S. E. Experimental and Molecular Modelling Studies of Overbased Detergent Particles. *Phys. Chem. Chem. Phys.* **2000**, *2*, 5197–5207.
- (4) Chen, Z.; Chen, F.; Chen, D. Universal Phase Transformation Mechanism and Substituted Alkyl Length and Number Effect for the Preparation of Overbased Detergents Based on Calcium Alkylbenzene Sulfonates. *Ind. Eng. Chem. Res.* **2013**, *52*, 12748–12762.
- (5) Kobylansky, E.; Mishchuk, O.; Ishchuk, Y. The Overbased Lubricating Grease: Regularities and Peculiarities of Properties. *Chem. Chem. Technol.* **2011**, *5*, 231–239.
- (6) Hudson, L. K.; Eastoe, J.; Dowding, P. J. Nanotechnology in Action: Overbased Nanodetergents as Lubricant Oil Additives. *Adv. Colloid Interface Sci.* **2006**, *123–126*, 425–431.
- (7) Bearchell, C. A.; Heyes, D. M.; Moreton, D. J.; Taylor, S. E. Overbased Detergent Particles: Experimental and Molecular Modelling Studies. *Phys. Chem. Chem. Phys.* **2001**, *3*, 4774–4783.
- (8) Bodnarchuk, M. S.; Heyes, D. M.; Dini, D.; Chahine, S.; Edwards, S. Self-assembly of Calcium Carbonate Nanoparticles in Water and Hydrophobic Solvents. *J. Phys. Chem. C* **2014**, *118*, 21092–21103.
- (9) Griffiths, J. A.; Heyes, D. M. Atomistic Simulation of Overbased Detergent Inverse Micelles. *Langmuir* **1996**, *12*, 2418–2424.
- (10) Bakunin, V.; Suslov, A.; Kuzmina, G.; Parenago, O.; Topchiev, A. Synthesis and Application of Inorganic Nanoparticles as Lubricant Components. *J. Nanopart. Res.* **2004**, *6*, 273–284.
- (11) Quigley, D.; Rodger, P. M. Free Energy and Structure of Calcium Carbonate Nanoparticles During Early Stages of Crystallization. *J. Chem. Phys.* **2008**, *128*, 221101–221104.
- (12) Nudelman, F.; Sonmezler, E.; Bomans, P. H. H.; de With, G.; Sommerdijk, N. A. J. M. Stabilization of Amorphous Calcium Carbonate by Controlling its Particle Size. *Nanoscale* **2010**, *2*, 2436–2439.
- (13) Liu, D.; Zhang, M.; Zhao, G.; Wang, X. Tribological Behavior of Amorphous and Crystalline Overbased Calcium Sulfonate as Additives in Lithium Complex Grease. *Tribol. Lett.* **2011**, *45*, 265–273.
- (14) Stott, F. H.; MacDonald, A. G. The Influence of Acid Strength on the Corrosive Wear of Grey Cast Irons in Oil-sulphuric Acid Mixtures. *Wear* **1988**, *122*, 343–361.
- (15) Fu, J.; Lu, Y.; Campbell, C. B.; Papadopoulos, K. D. Temperature and Acid Droplet Size Effects in Acid Neutralization of Marine Cylinder Lubricants. *Tribol. Lett.* **2006**, *22*, 221–225.
- (16) Hone, D. C.; Robinson, B. H.; Steytler, D. C.; Glyde, R. W.; Galsworthy, J. R. Mechanism of Acid Neutralization by Overbased Colloidal Additives in Hydrocarbon Media. *Langmuir* **2000**, *16*, 340–346.
- (17) Wu, R. C.; Campbell, C. B.; Papadopoulos, K. D. Acid-Neutralizing of Marine Cylinder Lubricants: Effects of Nonionic Surfactants. *Ind. Eng. Chem. Res.* **2000**, *39*, 3926–3931.
- (18) Wu, R. C.; Papadopoulos, K. D.; Campbell, C. B. Acid-neutralizing of Marine Cylinder Lubricants: Measurements and Effects of Dispersants. *AIChE J.* **2000**, *46*, 1471–1477.
- (19) Fu, J.; Papadopoulos, K. D.; Lu, Y.; Campbell, C. B. Ostwald Ripening: A Decisive Cause of Cylinder Corrosive Wear. *Tribol. Lett.* **2007**, *27*, 21–24.
- (20) Fu, J.; Lu, Y.; Campbell, C. B.; Papadopoulos, K. D. Acid Neutralization by Marine Cylinder Lubricants Inside a Heating Capillary: Strong/Weak-Stick Collision Mechanisms. *Ind. Eng. Chem. Res.* **2006**, *45*, 5619–5627.
- (21) Fernandez-Martinez, A.; Kalkan, B.; Clark, S. M.; Waychunas, G. A. Pressure-induced Polyamorphism and Formation of 'Aragonitic' Amorphous Calcium Carbonate. *Angew. Chem., Int. Ed.* **2013**, *52*, 8354–8357.
- (22) Bodnarchuk, M. S.; Heyes, D. M.; Dini, D.; Chahine, S.; Edwards, S. Role of Deprotonation Free-energies in pK_a Prediction and Molecule Ranking. *J. Chem. Theory Comput.* **2014**, *10*, 2357–2545.
- (23) Tomlinson, A.; Danks, T. N.; Heyes, D. M.; Taylor, S. E.; Moreton, D. J. Interfacial Characterization of Succinimide Surfactants. *Langmuir* **1997**, *13*, 5881–5893.
- (24) Malde, A. K.; Zuo, L.; Breeze, M.; Stroet, M.; Poger, D.; Nair, P. C.; Oostenbrink, C.; Mark, A. E. An Automated Force Field Topology Builder (ATB) and Repository: Version 1.0. *J. Chem. Theory Comput.* **2011**, *7*, 4026–4037.
- (25) Canzar, S.; El-Kebir, M.; Pool, R.; Elbassioni, K.; Mark, A. E.; Geerke, D. P.; Stougie, L.; Klau, G. W. Charge Group Partitioning in Biomolecular Simulation. *J. Comp. Biol.* **2013**, *20*, 188–198.
- (26) Tobias, D. J.; Klein, M. L. Molecular Dynamics Simulations of a Calcium Carbonate/Calcium Sulfonate Reverse Micelle. *J. Phys. Chem.* **1996**, *100*, 6637–6648.
- (27) Kohagen, M.; Mason, P. E.; Jungwirth, P. Accurate Description of Calcium Solvation in Concentrated Aqueous Solutions. *J. Phys. Chem. B* **2014**, *118*, 7902–7909.
- (28) Wang, J.; Becker, U. Structure and Carbonate Orientation of Vaterite. *Am. Mineral.* **2012**, *97*, 1424–1436.
- (29) Jain, A.; Jochum, M.; Peter, C. Molecular Dynamics Simulations of Peptides at the Air Water Interface: Influencing Factors on Peptide-Templated Mineralization. *Langmuir* **2014**, *30*, 15486–15495.
- (30) Skovbjerg, L. L.; Hassenkam, T.; Makovicky, E.; Hem, C. P.; Yang, M.; Bovet, N.; Stipp, S. L. S. Nano Sized Clay Detected on Chalk Particle Surfaces. *Geochim. Cosmochim. Acta* **2012**, *99*, 57–70.

- (31) Reischl, B.; Watkins, M.; Foster, A. S. Free Energy Approaches for Modeling Atomic Force Microscopy in Liquids. *J. Chem. Theory Comput.* **2013**, *9*, 600–608.
- (32) Van Der Spoel, D.; Lindahl, E.; Hess, B.; Groenhof, G.; Mark, A. E.; Berendsen, H. J. C. GROMACS: Fast, Flexible, and Free. *J. Comput. Chem.* **2005**, *26*, 1701–1718.
- (33) Pronk, S.; Páll, S.; Schulz, R.; Larsson, P.; Bjelkmar, P.; Apostolov, R.; Shirts, M. R.; Smith, J. C.; Kasson, P. M.; van der Spoel, D.; Hess, B.; Lindahl, E. GROMACS 4.5: A High-throughput and Highly Parallel Open Source Molecular Simulation Toolkit. *Bioinformatics* **2013**, *29*, 845–854.
- (34) Essmann, U.; Perera, L.; Berkowitz, M. L.; Darden, T.; Lee, H.; Pedersen, L. G. A Smooth Particle Mesh Ewald Method. *J. Chem. Phys.* **1995**, *103*, 8577–8593.
- (35) Migamoto, S.; Kollman, P. A. Settle: An Analytical Version of the SHAKE and RATTLE Algorithm for Rigid Water Models. *J. Comput. Chem.* **1992**, *13*, 952–962.
- (36) Hess, B.; Bekker, H.; Berendsen, H. J. C.; Fraaije, J. G. E. M. LINCS: A Linear Constraint Solver for Molecular Simulations. *J. Comput. Chem.* **1997**, *18*, 1463–1472.
- (37) Bussi, G.; Donadio, D.; Parrinello, M. Canonical Sampling Through Velocity Rescaling. *J. Chem. Phys.* **2007**, *126*, 014101.
- (38) Woodcock, L. V. Isothermal Molecular Dynamics Calculations for Liquid Salts. *Chem. Phys. Lett.* **1971**, *10*, 257–261.
- (39) Nosé, S. Constant Temperature Molecular Dynamics Methods. *Prog. Theor. Phys. Suppl.* **1991**, *103*, 1–46.
- (40) Parrinello, M.; Rahman, A. Polymorphic Transitions in Single Crystals: A New Molecular Dynamics Method. *J. Appl. Phys.* **1981**, *52*, 7182–7190.
- (41) Rudnick, J.; Gaspari, G. The Asphericity of Random Walks. *J. Phys. A: Math. Gen.* **1986**, *19*, L191–193.
- (42) Rudnick, J.; Gaspari, G. The Shapes of Random Walks. *Science* **1987**, *237*, 384–389.
- (43) Bearchell, C. A.; Heyes, D. M. Molecular Modelling Studies of Calcium Carbonate and its Nanoparticles. *Mol. Sim.* **2002**, *28*, 517–538.
- (44) Fernandez-Gonzalez, A.; Fernandez-Seivane, L.; Rubio, M. P.; Ferrer, J. A Molecular Study of CaCO₃ Cluster Configurations. arXiv:1105.5371, 2011. <http://arxiv.org/abs/1105.5371> (accessed May 5 2015).
- (45) Tegethoff, W. F. *Calcium Carbonate: From the Cretaceous Period into the 21st Century*; Birkhäuser: Basel, 2001.
- (46) Darkins, R.; Sushko, M. L.; Liub, J.; Duffy, D. M. Stress in Titania Nanoparticles: An Atomistic Study. *Phys. Chem. Chem. Phys.* **2014**, *16*, 9441.
- (47) Torrie, G. M.; Valleau, J. P. Nonphysical Sampling Distributions in Monte Carlo Free-energy Estimation: Umbrella Sampling. *J. Comput. Phys.* **1977**, *23*, 187–199.
- (48) Kumar, S.; Bouzida, D.; Swendsen, R. H.; Kollman, P. A.; Rosenberg, J. M. The Weighted Histogram Analysis Method for Free-energy Calculations on Biomolecules. I. The Method. *J. Comput. Chem.* **1992**, *13*, 1011–1021.
- (49) Clint, J. H.; Taylor, S. E. Particle Size and Interparticle Forces of Overbased Detergents: A Langmuir Trough Study. *Colloids Surf.* **1992**, *65*, 61–671.
- (50) Jiang, J.; Zhu, Y.; Cui, Z.; Binks, B. P. Switchable Pickering Emulsions Stabilized by Silica Nanoparticles Hydrophobized In Situ with a Switchable Surfactant. *Angew. Chem., Int. Ed.* **2013**, *14*, 12599–12602.
- (51) Fortini, A. Clustering and Gelation of Hard Spheres Induced by the Pickering Effect. *Phys. Rev. E* **2012**, *85*, 040401.
- (52) Bearchell, C. A.; Edgar, J. A.; Heyes, D. M.; Taylor, S. E. Dielectric Spectroscopic and Molecular Simulation Evidence for Aggregation of Surfactant-stabilized Calcium Carbonate Nanocolloids in Organic Media. *J. Colloid Interface Sci.* **1999**, *210*, 231–240.
- (53) Totten, G. E., Shah, R. J. *Fuels and Lubricants Handbook: Technology, Properties, Performance, and Testing*; ASTM: Glen Burnie, MA, 2003.
- (54) Rudnick, L. R. *Synthetics, Mineral Oils, and Bio-Based Lubricants: Chemistry and Technology*, 2nd ed.; CRC Press: Boca Raton, FL, 2013.